MINIATURE ANTENNAS & ARRAYS USING NOVEL MATERIALS

J. L. Volakis, C.-C. Chen, G. Mumcu and K. Sertel.
ECE Dept., ElectroScience Laboratory, The Ohio State University
1320 Kinnear Rd., Columbus, OH, 43212 USA.

I. INTRODUCTION

It is well-recognized that materials design is a new frontier in developing novel antennas that are smaller in size and integrate greater multi-functionality than ever before. This need is fueled by a multitude of new applications in commercial and military communications coupled with high data rate requirements. Indeed, engineered materials, such as new composites, electromagnetic bandgap and periodic structures have had strong interest in recent years due to their extraordinary and unique electromagnetic behavior [1]. As a result, an extensive literature on the theory and application of artificially modified materials has arisen. This overview paper will cover various methods for enhancing antenna and array properties, including material and shape design, novel and complex anisotropic materials for wave slow down, lumped loads for traveling wave antennas, reactive ground planes, and impedance matching techniques for extremely small antennas. Specifically, we will discuss how modified materials, (L,C) lumped loads and low loss magnetic materials/crystals (metamaterials) are impacting antenna design with the goal of overcoming miniaturization challenges (viz. bandwidth and gain reduction, multi-functionality etc.). Dielectric design and texturing has for example led to reducing UHF antenna size by more than a factor of 2-3 while retaining a 30% bandwidth and 4dBi gain for a 6" aperture. For broadband antennas, such as spirals, we found that a reactive ground plane with variable impedance, lumped reactive loads, dielectric tapering of the superstrate and substrate with low loss ceramics, and broadband impedance matching, all combined to achieve substantial miniaturization, particularly for antennas which are less than 0.2 wavelengths in diameters [2].

A portion of the presentation will focus on two new classes of photonic crystals (referred to as magnetic photonic crystals (MPCs) and degenerate band edge (DBE) crystals) for antenna and array applications. MPCs display spectral non-reciprocity and have been shown to exhibit some rather remarkable properties to be harnessed in antenna design. Among them is (a) drastic incoming wave slow down and (b) significant amplitude growth while (c) maintaining minimal reflection at the interface with free space [3] [4] [5]. These phenomena are associated with diverging frozen modes that occur around the stationary inflection points within the propagation band. Recently, we specifically considered the performance of small printed antennas embedded within the MPC structure and compared it with the performance of similar antennas in plain dielectric slabs. We showed that the excited frozen modes within the MPC contribute to a significant gain increase and narrow beamwidths [6] [7]. Further, we demonstrated array performance and scanning properties within the MPC using realistic materials [7].

The second class of crystals is based on the concept of degenerate band edge (DBE). As such, the band diagram of the crystal becomes relatively flatter at the band edge as compared to a regular band edge crystal (RBE) (see Fig. 1 (a)). A semi-infinite DBE slab is more matched at the interface, experiencing a higher transmittance ($\Delta\omega_d^{1/4}$), whereas the transmittance around the RBE vanishes with a rate of $\Delta\omega_d^{1/2}$ ($\Delta\omega_d$ is the difference between the band edge frequency and the frequency of operation). Also the group velocity decreases more quickly in the DBE crystals ($\Delta\omega_d^{3/4}$) as compared to the rate $\Delta\omega_d^{1/2}$observed in RBE crystals. The consequence of this behavior is a higher amplitude increase in the vicinity of the DBE. In this paper, we will first briefly discuss the amplitude increase in the DBE crystals. We will specifically place a small printed dipole within the DBE crystals to harness the concentrated field. We will then demonstrate how these antennas exhibit higher received power and narrow beamwidths as compared to the same antennas embedded in isotropic homogenous dielectric slabs.

II. AMPLITUDE INCREASE AROUND THE DBE

An important aspect of the DBE crystals is that they can be realized with readily available materials. The DBE structure that will be considered throughout the paper is made up of N unit cells, each consisting of two identical anisotropic dielectric layers, misaligned with respect to each other (A layers), and one free space layer (F layer) (see Fig. 1 (b) for the unit cell structure and material parameters).

In finite thickness crystals, the transmittance is associated with the Fabry–Perot resonances. The only way of realizing a slow mode in RBE or DBE crystals is to bring these resonances as close to the band edge as possible by keeping the

thickness of the crystal large enough. Since the transmittance of the DBE crystals is reduced more slowly as compared to the RBE crystals, the same amplitude increase can be achieved using fewer layers. In addition, the faster vanishing group velocity provides a better amplification factor for the DBE crystals. Also the possibility of large dielectrics can allow for significant antenna miniaturization. It is therefore important to discuss antenna miniaturization and gain enhancements within the DBE crystals.

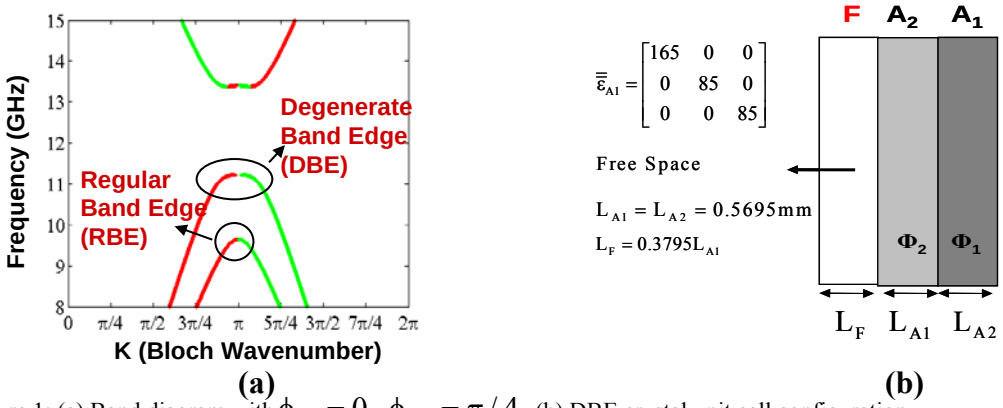

Figure 1: (a) Band diagram with $\phi_{A1} = 0$, $\phi_{A2} = \pi/4$. (b) DBE crystal unit cell configuration.

Before moving into antenna performance within DBE crystals, let us first consider the amplitude increase around DBE. To observe the effect of thickness and crystal orientation on amplitude increase, we investigate three different crystals. For the first case, the thickness of the crystal is taken to be N = 20 and misalignment angles are adjusted to be φ_{A1}=0 and φ_{A1}=π/4. In this case, the closest Fabry–Perot peak to the DBE occurs at 11.196GHz, and we specifically observe that $|E_x|$ and $|E_y|$ reach to amplitudes of 2.6 and 2.9, respectively inside the crystal. When the illumination is y–polarized, $|E_x|$ and $|E_y|$ attains amplitudes of 2.9 and 3.3. Depending on the application, it can be more desirable to make the crystal transparent to only one polarization. Fig. 2 (a) depicts the transmittance of the same DBE crystal (N = 20) when it is rotated by an angle of −3π/10 about its center axis. As clearly seen, the rotated crystal is almost transparent to the x–polarized incident field. Accordingly the maximum amplitudes achieved inside the DBE become 4.1 and 4.3 for |Ex| and |Ey|, respectively. The third DBE crystal consists of N = 10 unit cells and the misalignment angles are identical to the second case. The closest Fabry–Perot peak occurs at 11.036GHz and the maximum amplitudes inside the crystal becomes |Ex| = 1.8 and |Ey| = 2.2 for the x–polarization.

III. DIPOLE AND ARRAY PERFORMANCE IN THE DBE CRYSTAL

To demonstrate antenna miniaturization and directivity enhancement in DBE crystals, let us consider a very short strip dipole placed within the DBE crystals discussed in the previous section. For matching purposes, the length of the dipole is taken to be $0.065\lambda_0$ which is slightly larger than $0.05\lambda_0$ ($\lambda_0/20$) (λ_0 being the free space wavelength at the operation frequency). The width of the dipole was assumed to be approximately 10 times smaller ($0.005\lambda_0$) to emulate a wire dipole. We specifically choose the operating frequencies at the Fabry–Perot peaks closest to the DBE (11.196GHz for N = 20 and 11.036GHz for N = 10). The thicknesses of the crystals are only $0.93\lambda_0$ for the first two cases and $0.46\lambda_0$ for the last one. We placed the dipoles within the layers where the field attains its maximum value. Specifically, the location of the dipole for the first case was between the 11^{th} and 12^{th} unit cells. In the second case the dipole was placed at the end of the F layer in the 10^{th} unit cell. In the last case it was located at the end of the F layer of the 5^{th} unit cell. Since the average dielectric constant inside the crystal is around 100, we compared the dipole performance with the $0.05\lambda_0$ long dipole antenna embedded within an isotropic homogenous dielectric slab of $\varepsilon_r = 100$. Further, we chose the thickness of the slab to be $1\lambda_0$ and $0.5\lambda_0$ to allow for a perfect matching at normal incidence.

For modeling the dipole inside the crystal (and simple dielectric medium), we carried out a moment method (MoM) analysis using the spectral domain Green's function to model the multilayered media. The induced currents were found by using MoM with rooftop basis functions. As expected, a challenge in the numerical implementation was the anisotropic nature of the layers and existence of strongly evanescent waves. We specifically employed a recursive series approach to overcome numerical instabilities due to the latter case [8].

To obtain the received power by the $0.065\lambda_0$ dipole we calculated the open circuit voltage V_{OC} and short circuit current I_{SC}. The Thevenin equivalent circuit was then employed to calculate the power received at the load impedance Z_L.

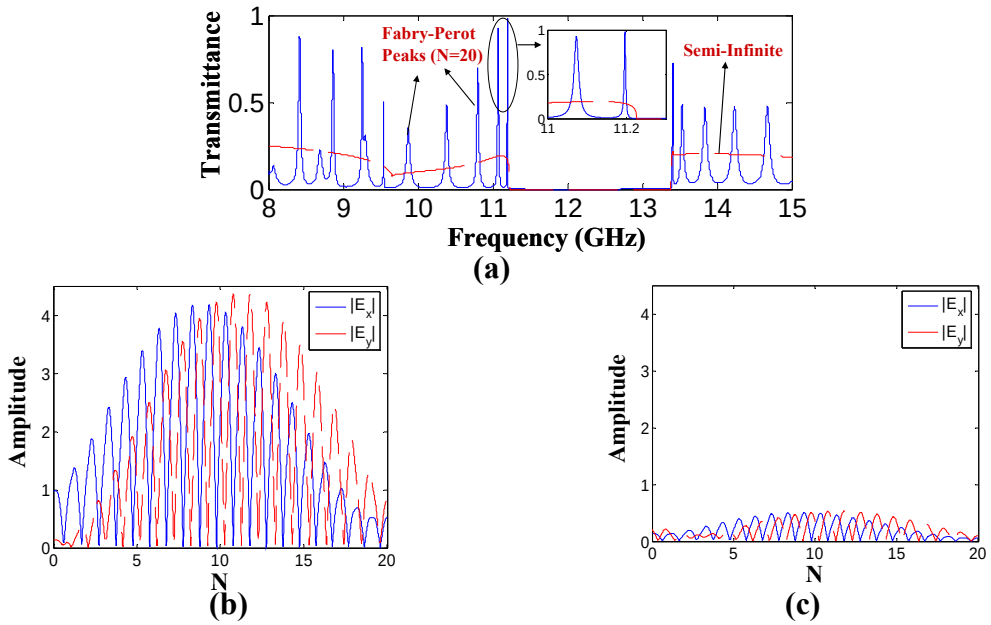

Figure 2: (a) Transmittance of the finite crystal for x-polarization, N=20, φ_{A1}=-3π/10, φ_{A2}=-π/20. $|E_x|$ and $|E_y|$ in the crystal for (b) x-polarized (c) y-polarized incident plane waves.

We first observed that the dipoles have very similar input impedances ($Z_{IN} = V_{OC}/I_{SC}$) for all three cases. Specifically, the input impedances were Z_{IN1} = 9.82 + 1.44j, Z_{IN2} = 10 + 1.7j, and Z_{IN3} = 10 + 1.8j for the three DBE crystal cases, respectively. In the simple slab the input impedances were Z_{IND1} = 10.85 + 3.5j and Z_{IND2} = 11.36 + 4.3j for $1\lambda_0$ and $0.5\lambda_0$ thicknesses, respectively. Since the input impedances of the dipoles are very close to each other, we compare the performance by matching the dipoles perfectly ($Z_L = Z_{IN}^*$). As expected, the amplitude increase inside the DBE crystal manifests itself in higher received power. Specifically, the dipole inside the first DBE crystal receives 9.4dB more power than the reference antenna in a simple medium when the crystal is illuminated with an x–polarized incident field (see Fig. 3 (a)). We also observe that the half power beamwidth of the dipole is greatly reduced inside the first DBE crystal (from 76^0 down to 10^0). This effect is a direct result of the band diagram sensitivity to the incidence angle. Since the k–ω diagram and the associated Fabry–Perot resonance peak move along the frequency axis as the incidence angle deviates from normal, the effect of amplification in the DBE crystal is only confined within a certain direction. For the second DBE crystal, the same dipole receives 12.7dB more power than the reference antenna in simple medium when the crystal is again excited by an x–polarized incident field. In addition, when the loss factors ($\tan\delta = 10^{-4}$) of the dielectric layers are taken into account, the dipole received power is reduced by only 1.9dB in both cases, that is the dipole displays almost the same performance in the low loss DBE crystal. When the dipole is placed inside the thin DBE crystal, the received power relative to the reference antenna drops as expected (see Fig. 4 (a)). Nevertheless, the dipole still receives 5.8dB more power (4.5dB more when lossy) over the reference antenna. Moreover the half power beamwidth of the dipole inside the DBE is also much narrower than the reference antenna (26^0 compared to 76^0). It is important to also investigate the performance of possible array configurations within these crystals. Of course, the miniature element size with enhanced directivity is promising for implementation of miniature superdirective arrays within DBE crystals. Fig. 4 (b) presents an example of an 11 element endfire array within the DBE crystal. The 11 elements of the array are 0.065 λ_0 dipoles and placed above and below the center element which itself is located at the end of F layer of the 10^{th} unit cell. Each element is separated a unit cell from each other with a linear phasing of -π in order to direct the beam along +z–direction (at the band edge, the phase difference across a unit cell is approximately -π). The load was matched to the normal incidence impedance. As seen from Fig. 4 (b), the endfire array allows for an additional 9.1dB increase in received power over the single element in the DBE crystal. Moreover, the side lobes of the receiving pattern are greatly suppressed as expected.

IV. CONCLUDING REMARKS

The unique propagation characteristics of DBE crystals are of great interest for antenna and array enhancements. Significant directivity increase is possible due to the dependence of the k–ω diagram on the angle of incidence. Accordingly, miniature elements with improved gain and directivity within these crystals are possible and this allows for the realization of miniature high gain antennas. Furthermore, endfire array configurations are of particular interest

for miniature super–gain antenna designs. Although our emphasis was on the receiving properties, the same conclusions can be made for radiating elements placed within DBE crystals using the reaction theorem. In conclusion, DBE crystals allow for drastic improvements in antenna radiation and receiving parameters, including gain, pattern, and size.

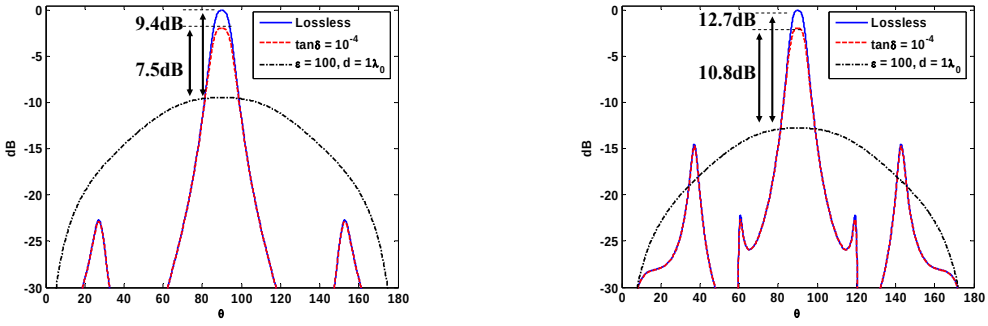

Figure 3: Dipole received power in the DBE crystal relative to that in the simple medium (a) $\varphi_{A1}=0$, $\varphi_{A2}=\pi/4$ (b) $\varphi_{A1}=-3\pi/10$, $\varphi_{A2}=-\pi/20$

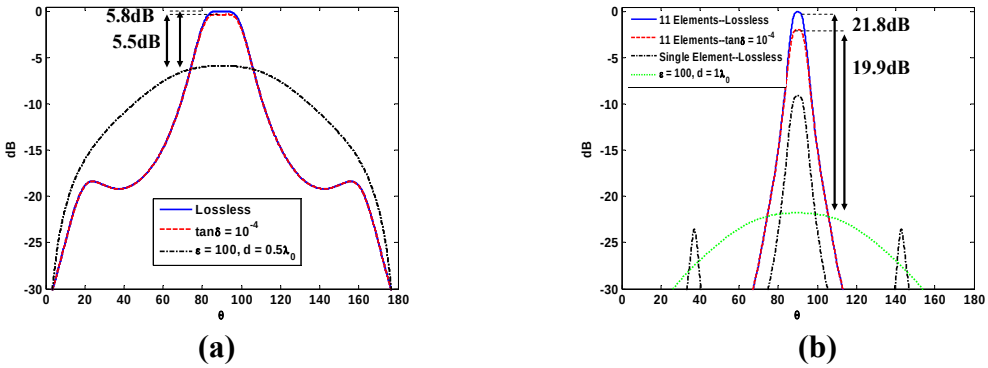

Figure 4: (a) Dipole received power in the DBE crystal relative to that in the simple medium, $\varphi_{A1}=-3\pi/10$, $\varphi_{A2}=-\pi/20$. (b) Received power by 11 element endfire array in DBE crystal, $\varphi_{A1}=-3\pi/10$, $\varphi_{A2}=-\pi/20$.

REFERENCES:

[1] IEEE Transactions on Antennas and Propagation, Special Issue on Metamaterials, vol. 51, Oct. 2003.

[2] J. L. Volakis, C. C. Chen, M. Lee, and B. Kramer, "Miniaturization methods for narrowband and ultrawideband antennas," in IEEE international workshop on antenna Technology: Small Antennas and Novel Metamaterials, Marina Mandarin, Singapore, Mar. 2005.

[3] A. Figotin and I. Vitebsky, "Nonreciprocal magnetic photonic crystals," Physical Review E, vol. 63, pp. 066 609,1–20, May 2001.

[4] A. Figotin and I. Vitebskiy, "Electromagnetic unidirectionality in magnetic photonic crystals," Physical Review B, vol. 67, pp. 165 210,1–20, Apr. 2003.

[5] G. Mumcu, K. Sertel, J. L. Volakis, A. Figotin, and I. Vitebsky, "RF propagation in finite thickness nonreciprocal magnetic photonic crystals," in Antennas and Propagation Society Symposium, 2004. IEEE, vol. 2, Monterey, California, June 2004, pp. 1395–1398.

[6] G. Mumcu, K. Sertel, and J. L. Volakis, "Miniature antennas & arrays embedded within magnetic photonic crystals," in EPFL Latsis Symposium, Lausanne, Switzerland, Mar. 2005.

[7] G. Mumcu, K. Sertel, and J. L. Volakis, "Superdirective miniature antennas embedded within magnetic photonic crystals," in submitted to 2005 IEEE AP-S International Symposium.

[8] W. C. Chew, Waves and Fields in Inhomogeneous Media, IEEE Press, New York, 1995.